JBC RESEARCH ARTICLE

Polyphosphates induce amyloid fibril formation of α-synuclein in concentration-dependent distinct manners

Received for publication, January 28, 2021, and in revised form, March 1, 2021 Published, Papers in Press, March 4, 2021,
https://doi.org/10.1016/j.jbc.2021.100510

Keiichi Yamaguchi[1,2], Masatomo So[2], César Aguirre[2,3], Kensuke Ikenaka[3], Hideki Mochizuki[3], Yasushi Kawata[4], and Yuji Goto[1,2,*]

From the [1]Global Center for Medical Engineering and Informatics, [2]Institute for Protein Research, [3]Department of Neurology, Graduate School of Medicine, Osaka University, Osaka, Japan; [4]Department of Chemistry and Biotechnology, Graduate School of Engineering, Tottori University, Tottori, Japan

Edited by Paul Fraser

Polyphosphates (polyPs), chains of phosphate residues found in species across nature from bacteria to mammals, were recently reported to accelerate the amyloid fibril formation of many proteins. How polyPs facilitate this process, however, remains unknown. To gain insight into their mechanisms, we used various physicochemical approaches to examine the effects of polyPs of varying chain lengths on ultrasonication-dependent α-synuclein (α-syn) amyloid formation. Although orthophosphate and diphosphate exhibited a single optimal concentration of amyloid formation, triphosphate and longer-chain phosphates exhibited two optima, with the second at a concentration lower than that of orthophosphate or diphosphate. The second optimum decreased markedly as the polyP length increased. This suggested that although the optima at lower polyP concentrations were caused by interactions between negatively charged phosphate groups and the positive charges of α-syn, the optima at higher polyP concentrations were caused by the Hofmeister salting-out effects of phosphate groups, where the effects do not depend on the net charge. NMR titration experiments of α-syn with tetraphosphate combined with principal component analysis revealed that, at low tetraphosphate concentrations, negatively charged tetraphosphates interacted with positively charged "KTK" segments in four KTKEGV repeats located at the N-terminal region. At high concentrations, hydrated tetraphosphates affected the surface-exposed hydrophilic groups of compact α-syn. Taken together, our results suggest that long-chain polyPs consisting of 60 to 70 phosphates induce amyloid formation at sub-μM concentrations, which are comparable with the concentrations of polyPs in the blood or tissues. Thus, these findings may identify a role for polyPs in the pathogenesis of amyloid-related diseases.

Currently, more than 35 types of proteins and peptides are known to form amyloid fibrils, which are misfolded ordered and linear aggregates associated with amyloidosis (1–3). Recent advances in solid-state NMR and cryo-EM revealed the cross-β-dominated atomic structures of many amyloid fibrils (3–6), confirming that they are indeed misfolded ordered structures achieved by hydrophobic interactions, hydrogen bonds, and van der Waals interactions, which also stabilize the globular native structures. Although folding and amyloid formation are alternative reactions of unfolded proteins (7, 8), the thermodynamic mechanisms of amyloid formation starting from native, denatured, or unfolded proteins remain unclear.

A traditional view is that amyloid fibrils are crystal-like aggregates of denatured proteins, which are formed above solubility upon breaking supersaturation (9–11). Supersaturation is a fundamental phenomenon of nature, determining the phase transition of substances. It is required for the formation of crystals and involved in numerous phenomena, *e.g.*, the supercooling of water prior to ice formation. The same is true for crystal-like amyloid fibrils. An additional trigger (*e.g.*, ultrasonic agitation) can disrupt supersaturation, leading to amyloid formation (11–13). We consider this traditional view, which should be combined with the atomic structures, to be important for advancing our understanding of amyloid formation.

Thus far, the effects of several additives, *i.e.*, salts (14), lipids (15–18), and metals (19), have been investigated and can be interpreted in terms of additive-dependent changes in solubility (18). Recently, among different additives, the role of polyphosphates (PolyPs) (Fig. 1*A*) consisting of high-energy phosphate anhydride-bonded inorganic phosphate has been focused on. PolyPs are one of the most ancient and conserved molecules in biology and are found in all prokaryotic and eukaryotic organisms (20, 21). Synthesized *in vivo* from ATP, these molecules exhibit a number of different functions. In bacteria, polyPs mainly serve as an energy store and a reserve pool of inorganic phosphate (22), whereas in eukaryotes, they have been implicated in the stimulation of blood coagulation (23), regulation of mitochondrial ion transport (24), energy metabolism (25), macrophage inflammatory response (26), *etc.* Cremers *et al.* (27) reported that polyPs accelerate the amyloid formation of several proteins, including α-synuclein (α-syn). We also reported that polyPs significantly induce amyloid formation of β_2-microglobulin, a protein responsible for dialysis-related amyloidosis, at both acidic and neutral pH (28). More recently, Wang *et al.* (29) reported that medium-chain-

* For correspondence: Yuji Goto, gtyj8126@protein.osaka-u.ac.jp.

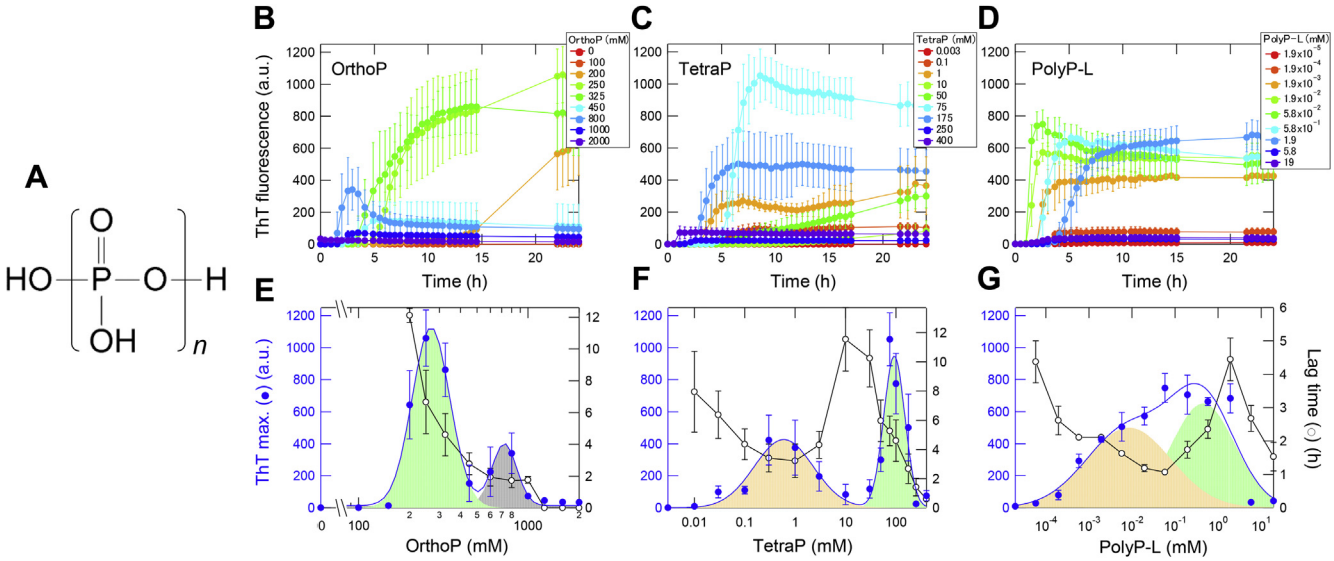

Figure 1. Amyloid formation of α-syn in the presence of different kinds of polyPs. *A*, chemical structure of polyP. *n* is the degree of polymerization of the phosphate group. *B–D*, kinetics of amyloid formation monitored by ThT fluorescence at varying concentrations of orthoP (*B*), tetraP (*C*), and polyP-L (*D*). The concentrations of polyPs are shown in the figures. *E–G*, maximum values of ThT fluorescence (*blue*) and lag times (*black*) in the presence of orthoP (*E*), tetraP (*F*), and polyP-L (*G*). Each point and bar represent the average and standard deviation of five independent experiments, respectively. Maximum values of ThT fluorescence in Figures 1 and 2 were fitted with three Gaussian curves including the charge–charge interactions (*orange*), Hofmeister salting-out effects (*green*) and higher unknown component (*gray*).

length polyP (60-mer) induced the liquid–liquid phase separation of green fluorescent protein *in vivo* and *in vitro*. Thus, polyPs may play numerous roles in protein aggregation and related phenomena (30, 31).

We examined the effects of polyPs of varying chain length on α-syn amyloid formation, revealing two concentration regions of amyloid acceleration. The lower and higher polyP concentrations promoted amyloid formation by attractive charge–charge interactions between positive groups of α-syn and negative polyPs and Hofmeister salting-out effects, respectively. As the former occurs at polyP concentrations comparable with those *in vivo*, polyPs are likely to play important roles in the pathogenesis of amyloid-related diseases. This study extends the view of amyloid formation on the basis of solubility and supersaturation.

Results

PolyP-induced amyloid formation of α-syn

We examined the amyloid formation of α-syn in the presence of polyPs with varying chain lengths: orthophosphate (orthoP), diphosphate (diP), triphosphate (triP), tetraphosphate (tetraP), short polyphosphate consisting of 10 to 15 phosphates (polyP-S) and long polyphosphate consisting of 60 to 70 phosphates (polyP-L) (Fig. 1 and Fig. S1). The concentration of α-syn (0.1 mg/ml, 6.9 μM) used in this study was comparable with that in neuronal cells (32) and was lower than those used in previous studies (0.5–1 mg/ml) (14, 19, 33, 34).

At 0 to 100 mM orthoP, the thioflavin T (ThT) fluorescence did not increase during an incubation of 24 h (Fig. 1*B*). According to the solubility and supersaturation mechanism, the solubility of α-syn was higher than 0.1 mg/ml. At 200 to 325 mM orthoP, the ThT fluorescence increased markedly after a lag time of several hours, suggesting that the solubility decreased below 0.1 mg/ml. However, at concentrations higher than 450 mM orthoP, the ThT fluorescence did not increase, when amorphous aggregates were likely to be formed (see below). The profile of diP-dependent acceleration and inhibition was similar to that of orthoP, although the concentrations to induce amyloid formation (100–200 mM) were lower than those of orthoP (Fig. S1*A*). For other polyPs with higher phosphate numbers, we observed more complicated profiles with an additional region of acceleration at the lower concentrations (Fig. 1, *C* and *D* and Fig. S1, *B* and *C*).

By fitting the ThT profiles observed for different polyPs to Gaussian curves, we determined the optimal concentrations for amyloid formation (Fig. 1, *E–G* and Fig. S1, *F–H*). As for orthoP, the optimal concentration for the major peak was approximately 270 mM and the minor peak, which was likely to be caused by amorphous aggregation (see below), had an optimum at 700 mM (Fig. 1*E*). The optimal concentration for orthoP was slightly lower than that of NaCl (~830 mM) (Fig. S1, *D* and *I*).

The optimal ThT concentrations of polyPs corresponding to the major orthoP peak were 110 mM triP, 92 mM tetraP, 3.6 mM polyP-S, and 4.5×10^{-1} mM polyP-L (Fig. 1 and Fig. S1), demonstrating that the optimal concentration deceased slightly with an increase in the phosphate number (Fig. 2). On the other hand, the second ThT optimal concentrations were 7.3 mM triP, 5.9×10^{-1} mM tetraP, 9.9×10^{-2} mM polyP-S, and 8.5×10^{-3} mM polyP-L (Fig. 1, *F* and *G* and Figs. S1, *G* and *H*), suggesting that the second optimum concentration decreased markedly with an increase in the phosphate number (Fig. 2). The lag time exhibited a pattern slightly opposite to that of ThT fluorescence (Fig. 1 and

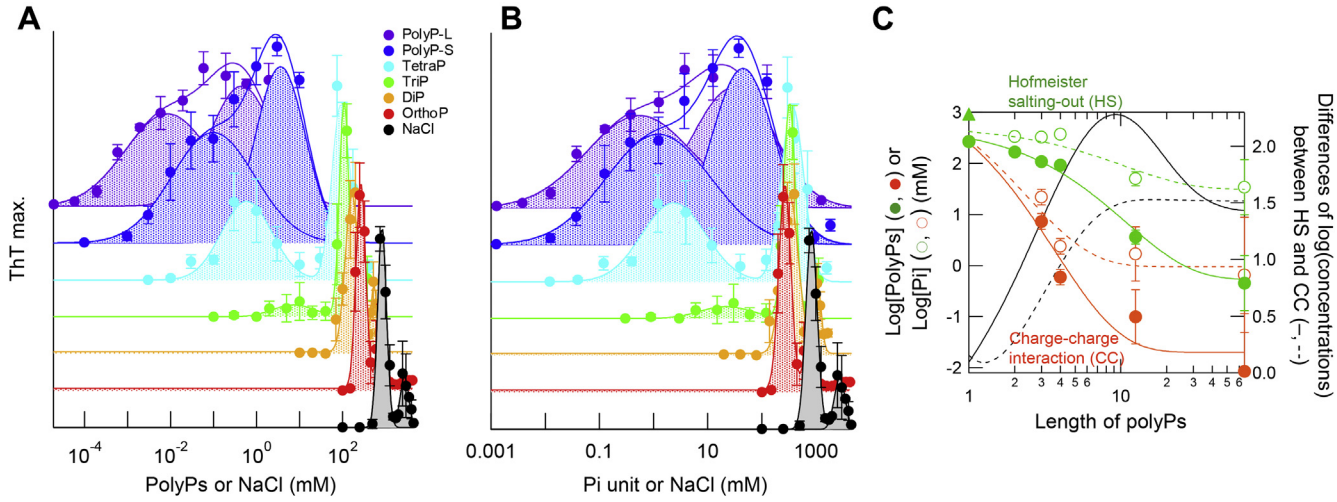

Figure 2. PolyP concentration dependency of the amyloid formation of α-syn. *A* and *B*, amyloid formation in the presence of varying chain lengths and concentrations of polyPs plotted against polyP or NaCl concentrations (*A*), or phosphate unit or NaCl concentrations (*B*). Types of polyPs are shown in the figures. Data for orthoP, tetraP, and polyP-L are reproduced from Figure 1. *C*, logarithmic plots of optimal amyloid concentrations, which are caused by the charge–charge interactions (*orange*) and Hofmeister salting-out effects (*green*), obtained using the polyP concentration (*closed circles*), phosphate unit concentration (*open circles*), and NaCl concentration (*closed triangles*).

Fig. S1). Small peaks at higher additive concentrations were observed for orthoP, diP, and NaCl at 730, 540, and 2800 mM, respectively (Fig. 1*E* and Fig. S1, *F* and I; gray). These peaks were likely to be caused by the formation of amorphous aggregates based on transmission electron microscopy (TEM) (Fig. 3 and Fig. S5).

To focus on the two regions of amyloid formation, we also plotted the maximum ThT fluorescence for different polyPs against the phosphate unit number (Fig. 2*C*). In addition, the differences between the two optimal concentrations were plotted against the phosphate unit number (Fig. 2*C*). The plot in terms of polyP molar concentrations, which emphasizes the electrostatic interactions, exhibited the maximal separation of two peaks for polyPs with ten phosphate units. On the other hand, the plot in terms of phosphate unit molar concentration suggested a moderate dependence of the high polyP-concentration peak on the phosphate number. The slope at midpoint was –4.3 mM log[PolyP]/log[Length of polyP] for the charge–charge interactions (*orange solid line*) and –2.2 mM log[PolyP]/log[Length of polyP] for the Hofmeister salting-out effects (*green solid line*). These distinct slopes were consistent with a view that the electrostatic attractions and general salting-out effects are involved in amyloid formation at low and high polyP concentrations, respectively (see below). The results also argue the usefulness of using both polyP molar concentration and phosphate unit molar concentration to address the mechanism of polyP effects.

Conformation and morphology of the α-syn aggregates

The far-UV circular dichroism (CD) spectra after amyloid formation monitored by ThT fluorescence confirmed β-sheet-rich amyloid fibrils in the range of 200 to 1000 mM orthoP (Fig. S2*A*). However, almost no CD signal was observed at 2000 mM orthoP, suggesting the formation of amorphous aggregates. For other polyPs (*i.e.*, diP, triP, tetraP, polyP-S, and polyP-L) and NaCl, the CD spectra exhibited β-sheet-rich conformations upon amyloid formation monitored by ThT fluorescence (Fig. S2, *B*–*G*).

We plotted the CD ellipticities at 203 nm and 218 nm against the concentrations of polyPs and NaCl (Fig. S3, *A*–*G*). In the presence of orthoP, the CD ellipticity at 218 nm negatively increased and that at 203 nm positively increased accompanied by an increase in ThT fluorescence (Fig. S3*A*). Similar dependencies were observed for diP, triP, tetraP, polyP-S, polyP-L, and NaCl (Fig. S3, *B*–*G*). However, the second transition at high polyP concentrations specifically increased the intensity at 203 nm, which was most clearly observed for polyP-S and polyP-L. This suggested that the secondary structures are slightly different between amyloid fibrils induced at low and high polyP concentrations.

By scrutinizing all of the TEM images obtained under various conditions (Fig. 3 and Fig. S4), we assessed the distinct morphologies of amyloid fibrils. In the presence of 250 mM orthoP, thick amyloid fibrils with diameters of ∼20 nm were observed by TEM (Fig. 3 and Fig. S4). These thick amyloid fibrils were also observed at higher concentrations of polyPs (*i.e.*, 100 mM tetraP or 0.58 mM polyP-L (Fig. 3 and Fig. S4), 200 to 525 mM diP, 125 mM triP, 3 mM polyP-S, or 750 mM NaCl (Fig. S5*A*)). In contrast, thin fibrils were observed at lower concentrations of polyPs (*i.e.*, 1 mM tetraP or 1.9×10^{-3} mM polyP-L (Fig. 3 and Fig. S4), 10 mM TriP or 3×10^{-2} mM polyP-S (Fig. S5*A*)). Of note, two types of amyloid fibrils of α-syn were previously reported to form at high and low NaCl concentrations, respectively (35, 36), consistent with the current results. In this paper, we also found that α-syn formed two types of fibrils (thin and thick fibrils) depending on the concentrations of polyP (Fig. 3 and Fig. S4). However, both of these fibrils were end products without conversion to each other.

Interactions of tetraP and α-syn analyzed by NMR

To address the interactions between polyPs and α-syn at the residue level, we measured the ^{1}H-^{15}N HQSC spectra of α-syn

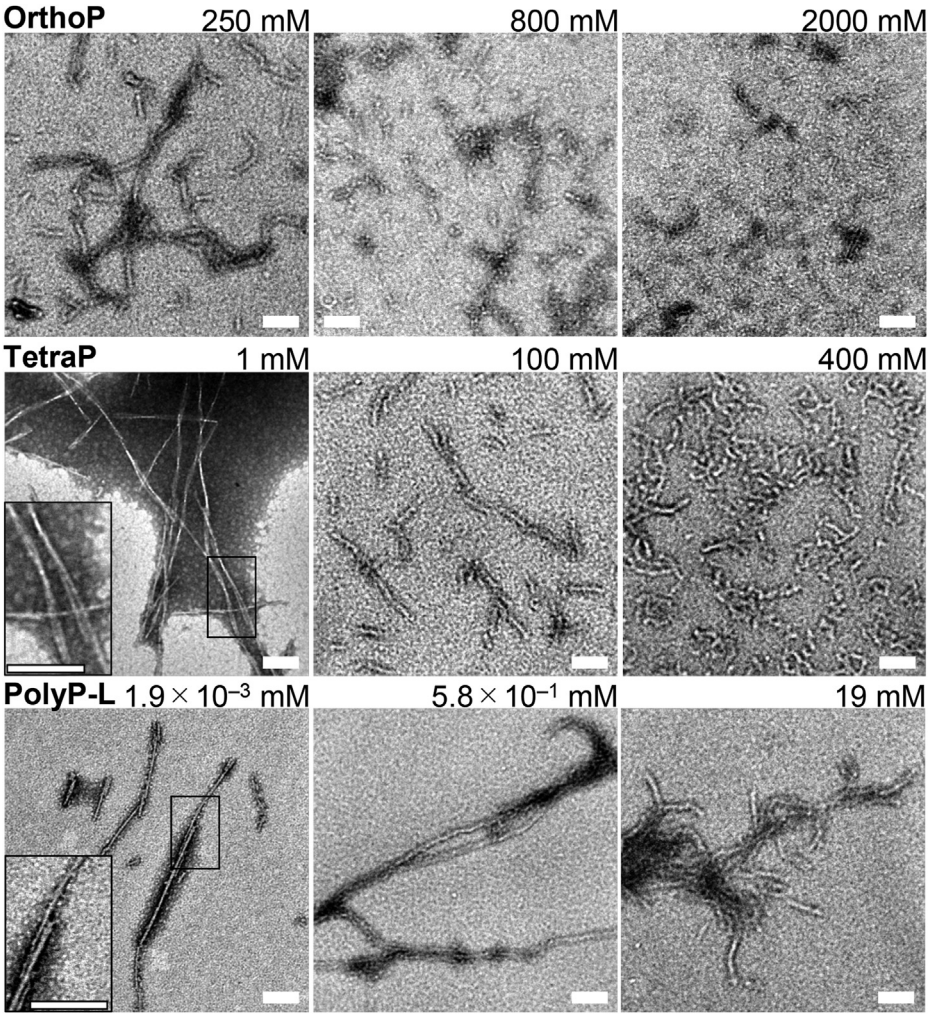

Figure 3. TEM images of α-syn aggregates in the presence of varying concentrations of polyPs. *Top*, orthoP, (*middle*) tetraP, and (*bottom*) polyP-L. The scale bars are 100 nm. *Insets* show the enlarged images of *square regions*.

at varying concentrations of tetraP (Fig. 4*A* and Fig. S6, *A* and *B*). Figure 4*A* was separated to Fig. S6, *A* and *B* to clarify the complicated movements of respective peaks depending on the tetraP concentration. We used tetraP because the low and high concentration regions of amyloid formation were most highly separated. We performed the NMR measurements at 15 °C following that so far the NMR experiments of α-syn were done at 15 °C under the neutral conditions (2) because of the fast exchange of amide protons with water at the higher temperature. In addition, for the NMR measurements, amyloid formation of α-syn should be suppressed during an incubation of several hours for the HSQC measurements and for longer periods including those for peak assignments. We confirmed the suppression of amyloid formation at the concentrations of 0 to 200 mM tetraP during an incubation of 24 h at 15 °C (Fig. S1, *E* and *J*). The experiments at 15 °C also showed that the amyloid formation occurred at 300 or 475 mM tetraP within several hours, suggesting that the peak tetraP concentrations caused by Hofmeister effects shifted to higher tetraP concentrations.

Signal assignments for 85% of the amino acid residues of α-syn were achieved at varying concentrations of tetraP. Some cross-peaks gradually shifted and curved trajectories were observed upon an increase in tetraP concentrations, suggesting at least two steps for the interaction of α-syn with tetraP. In particular, Ser and Thr residues, *i.e.*, S9, T22, T33, T44, and T81, shifted in the opposite direction between 0 and 5 mM and 5 and 100 mM tetraP (Figs. 4, *B* and *C* and 5*D*).

To determine the number of conformational states of soluble α-syn at different tetraP concentrations, principal component analysis (PCA) was performed using HSQC chemical shift data. PCA is a multivariate analysis used to simplify the complexity in high-dimensional data by geometrically projecting data onto lower dimensions called principal components (PCs) (37–39). As a result of PCA using the normalized chemical shift data, we obtained nine PCs, corresponding eigenvalues, and contribution ratios (Fig. 5*B*). The accumulative contribution ratio of PC1 was 0.58 and that of the first two PCs was 0.88. The plot of PC contribution ratios against the tetraP concentration revealed that PC1 and PC2

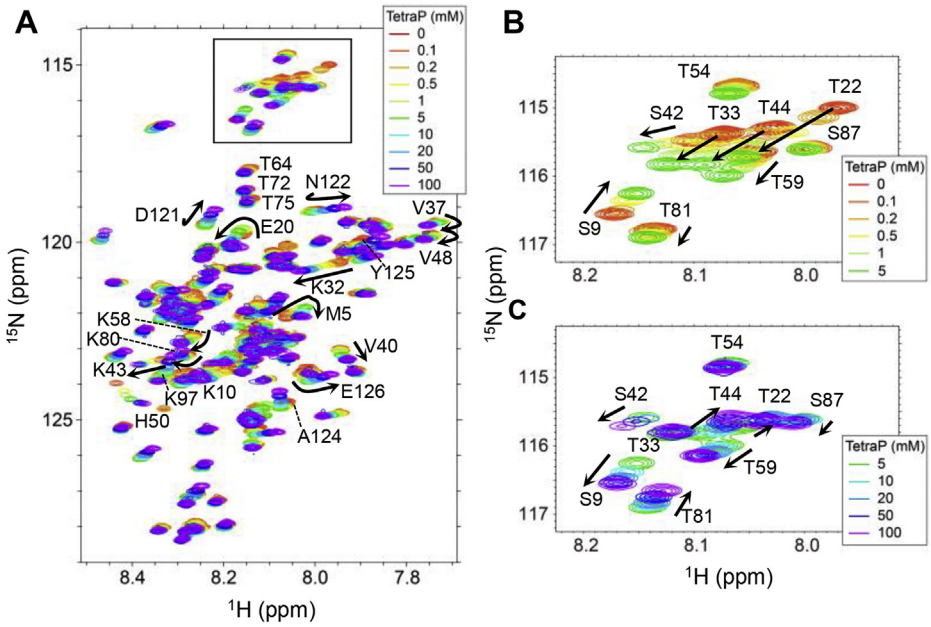

Figure 4. ^{1}H-^{15}N HSQC spectra of α-syn in the presence of varying concentrations of tetraP (*A*). Representative amino acid residues with a large shift are indicated in the figure. *B* and *C*, enlarged images of the enclosed area in the figure (*A*) at the concentrations of 0 to 5 (*B*) and 5 to 100 mM tetraP (*C*).

changed smoothly against the tetraP concentration, whereas PC3 was relatively low in intensity over the tetraP concentrations examined (Fig. S6*C*). Thus, two dominant PCs were sufficient to describe most of the observed signal movements.

The chemical shift perturbation (CSP) observed upon addition of tetraP could be potentially indicative of either (i) specific interactions between tetraP and α-syn or (ii) a backbone conformational change induced in α-syn due to the interaction with tetraP or (iii) due to the tetraP-dependent formation of soluble α-syn oligomers/aggregates. Although the observed chemical shift data may include these effects, PCA could not distinguish them at this stage. We then focused on the three different tetraP concentrations and obtained the stepwise differences among them in terms of PC contribution ratios (Fig. 5*C*): (i) 0 to 0.2 mM at which the contribution of PC1 was predominant, (ii) 0.2 to 5 mM at which the contribution of PC1 decreased and PC2 contribution was predominant, and (iii) 5 to 100 mM at which the negative contribution of PC1 was larger than that of PC2. The concentrations of (ii) and (iii) were approximately consistent with those to induce amyloid fibrils at low and high polyP concentrations, respectively (Figs. 1 and 2).

CSP demonstrated that the entire region of α-syn remained almost unchanged upon increasing tetraP concentration from 0 to 0.2 mM (Fig. 5, *D* and *E*). From 0.2 to 5 mM tetraP, CSP was observed, especially for T22, T33, T44, and T59 located in the N-terminal KTKEGV repeats and H50 residue (Fig. 5*F*). His residue may shift upon a slight change in solution pH around neutral pH (40). The Thr residues located in KTKEGV repeats were sandwiched between two Lys residues (Fig. 5*A*). CSPs of Lys residues on either or both sides of T22, T33, T44, and T59 were also observed. TetraP used in the NMR experiments is flexible and ∼10 Å in length because the high-energy phosphate bond (P–OP) is around 1.5 to 1.6 Å (41). The main chain of Thr residues may interact with tetraP through the "KTK" segment in KTKEGV repeats. In addition, the CSPs were observed at S9 located in the primary KTKEGV repeats and at around E126 in the C-terminal region (Fig. 5*F*). This suggested that the negatively charged tetraPs specifically bind to positively charged "KTK" segments in KTKEGV repeat motifs *via* charge–charge interactions, which may interfere with interactions between the N- and C-terminal regions of α-syn, as previously observed (42, 43). The N-terminal and NAC regions take a compact conformation, leading to the formation of amyloid fibrils (Fig. 6).

From 5 to 100 mM tetraP, CSPs were observed in the N and C terminals or the relatively hydrophilic regions of α-syn (Fig. 5*G*). Among them, large CSPs were observed at around K97, N122, and Y125. Thus, at the higher concentrations of 5 to 100 mM tetraP, hydrated tetraP affected chemical shifts of the N and C terminals or the relatively hydrophilic regions of α-syn by the preferential hydration of anions (Fig. 6). This is energetically unfavorable, leading to a conformational transition to a more compact and less surface-exposed structure, *i.e.*, amyloid fibrils (28, 44–46). NAC regions may become compact after the first optimum of amyloid formation and may not be affected by the high concentrations of tetraP.

Discussion

Molecular basis of two optimal concentrations

Two regions of amyloid formation dependent on additive concentrations were also observed for the heparin-dependent amyloid formation of hen egg white lysozyme (HEWL) at pH 2.0 and 60 °C (45), where HEWL and heparin are positively and negatively charged, respectively. They were also observed for polyP-dependent amyloid formation of β2-microglobulin at pH 7.0, where β2-microglobulin and polyP are both negatively

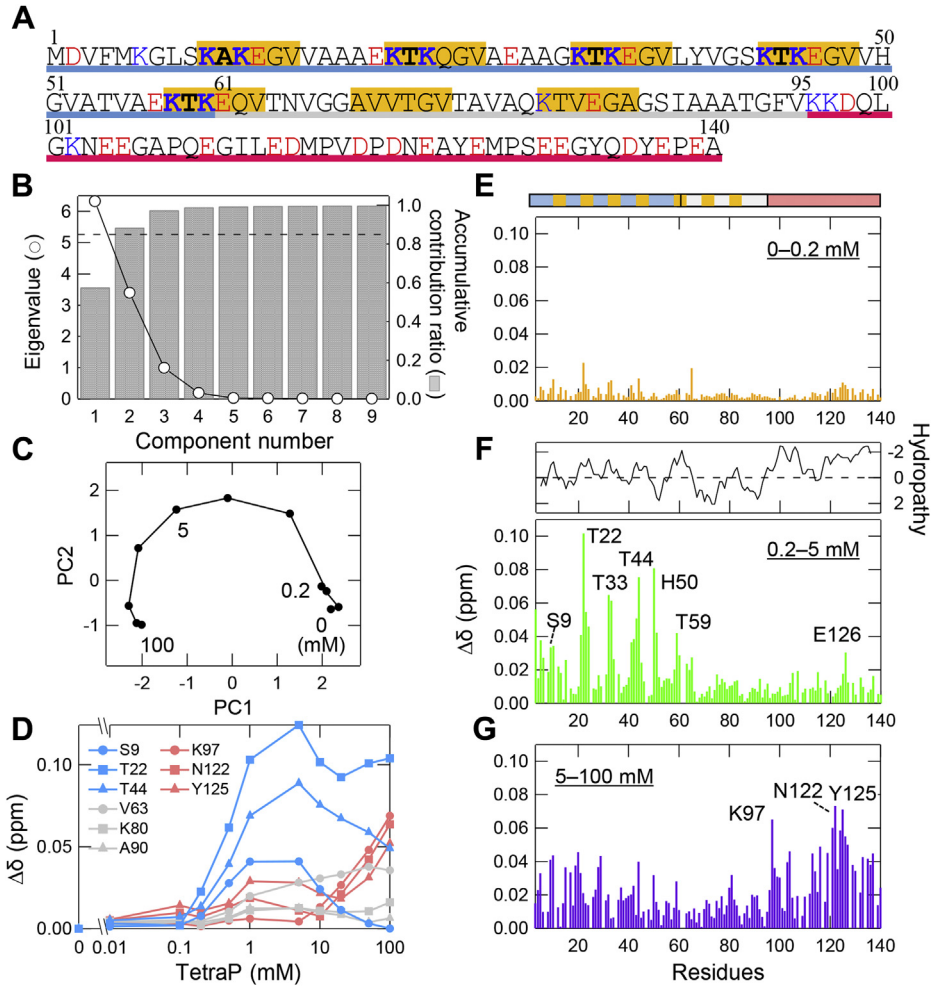

Figure 5. Interactions between tetraP and α-syn analyzed by NMR. *A*, amino acid sequence of α-syn, where the N-terminal, NAC, and C-terminal regions are *underlined* by *blue*, *gray*, and *red*, respectively, and "KTKEGV" repeat motifs are marked with *orange*. At pH 7.5, the positively and negatively charged residues are shown by *blue* and *red*, respectively. *B* and *C*, PCA of the NMR data against tetraP concentrations. *B*, the eigenvalues (*circles*) and accumulative contribution ratio (*bars*) of PCA. The *dashed line* indicates an accumulative contribution ratio of 0.85. *C*, the change in PC 1 and 2 scores depending on the tetraP concentrations. *D*, representative CSPs of HSQC peaks as a function of the molar concentration of tetraP. Colors correspond to the N-terminal (*light blue*), NAC (*gray*), and C-terminal (*pink*) regions, and their amino acid residues are shown in the figure. *E–G*, the CSPs between 0 and 0.2 mM (*E*), 0.2 and 5 mM (*F*), and 5 and 100 mM (*G*). The *bar above panel* (*E*) shows the sequence motifs of α-syn, with the same colors as those used in (*A*). Panel (*F*) also shows the hydropathy plot of α-syn against the residue number (60).

charged (30). Amyloid formation at the lower concentrations was explained in terms of the attractive charge–charge interactions between the positively charged proteins or regions and negatively charged polyPs. On the other hand, amyloid formation at the higher concentrations was explained in terms of the general salting-out effects (*i.e.*, Hofmeister salting-out effects), where the effects do not depend on the net charge but on the concentrations of active groups (*i.e.*, sulfate or phosphate groups). Water structure-making kosmotropic ions (*e.g.*, SO_4^{2-} and HPO_4^{2-}) exhibited stronger effects on protein folding or aggregation than water structure-breaking chaotropic ions (*e.g.*, SCN^- and ClO_4^-) (47, 48). Preferential hydration of unfolded proteins by hydrated anions is considered unfavorable in terms of free energy, leading to folding or amyloid formation with a decrease in exposed surface area. The stronger dependence on polyP length at the low concentration region than that at the high concentration region was consistent with a view that the electrostatic attractions and general salting-out effects are involved in amyloid formation at low and high polyP concentrations, respectively (Fig. 2*C*).

Moreover, for the amyloid formation of α-syn, counter anion binding and Hofmeister salting-out effects were suggested to be responsible at low and high pH conditions, respectively (14). For the amyloid formation of islet amyloid polypeptide, it was previously reported that, at pH 8.0, counter anion binding and Hofmeister salting-out effects are important at low and high salt concentrations, respectively (49). We recently reported that isoelectric point precipitation, the most traditional approach for precipitating proteins, effectively induced amyloid formation of α-syn at pH 4.7, its isoelectric point, under low-salt conditions (50). Taken together, amyloid fibrils are formed under numerous conditions where the solubility of unfolded proteins decreases, consistent with the solubility and supersaturation-dependent mechanism.

The two polyP-dependent regions of α-syn amyloid formation at pH 7.5 can be explained by the same mechanism. The

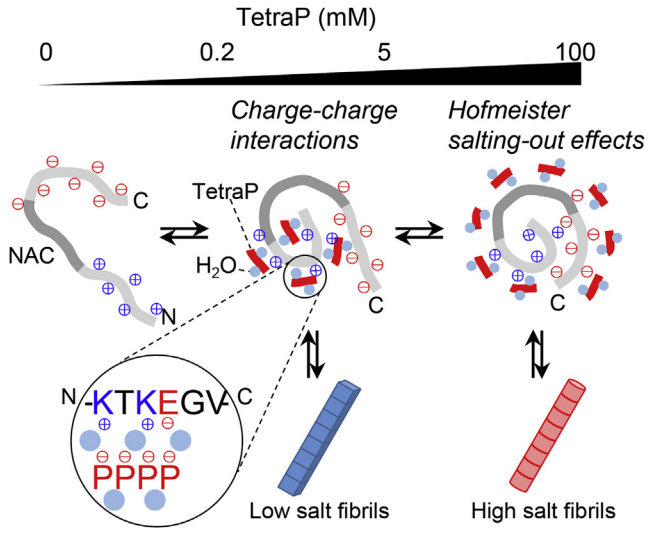

Figure 6. Schematic of the mechanisms for polyP-induced amyloid formation of α-syn at pH 7.0. α-Syn with a pI of 4.7 has a net charge of −10 at pH 7.0. In the absence of tetraP or salts, the negative net charge causes the extended α-syn conformation, although the positive and negative charges are clustered on the N- and C-terminal regions, respectively. At the lower concentrations of tetraP, negatively charged tetraPs interact with positively charged "KTK" segments in KTKEGV repeat motifs *via* charge–charge interactions. Shielding of the charge repulsions leads to compact NAC regions stabilized by hydrophobic interactions and the formation of low-salt amyloid fibrils. At higher concentrations of tetraP, hydrated tetraPs cause Hofmeister salting-out effects and lead to the formation of high salt amyloid fibrils, in which tetraPs affect surface-exposed protein-charged groups of compact monomers.

amino acid sequence of α-syn is divided into three regions: the positively charged N-terminal, middle hydrophobic NAC (amino acids 61–95), and negatively charged C-terminal regions (Fig. 5*A*), and it contains seven imperfect repeats with the KTKEGV consensus sequence (Fig. 5*A*; *orange*). Although the net charge of α-syn at pH 7.5 is −9, it has many positive charges, mostly at the N-terminal region. These positive charges are likely to interact with negative charges of polyPs, leading to the amyloid formation at low polyP concentrations. On the other hand, Hofmeister salting-out effects occur at high polyP concentrations. Electrostatic interactions and Hofmeister salting-out effects were focused on by plotting the molar polyP and phosphate unit concentrations, respectively (Fig. 2).

Role of polyP in synucleinopathy

In rodent tissues, polyP concentrations are between 25 and 120 μM in phosphate units, with an average length of 50 to 800 phosphate units (20), and in human platelets, polyPs consisting of 70 to 75 phosphates were identified at a concentration of 1.1 mM in phosphate units (51). In this study, the amyloid formation of α-syn at pH 7.5 was investigated in the presence of polyPs of varying chain lengths. PolyPs with more than three phosphate groups exhibited two optimal concentrations for amyloid formation, low and high concentration, which were caused by the charge–charge interactions and Hofmeister salting-out effects, respectively. Of note, long-chain polyP consisting of 60 to 70 phosphates induced amyloid formation by the charge–charge interactions at a sub-μM concentration, comparable with the concentration of polyP in the blood. Thus, the negatively charged multivalent biopolymers including polyP may play an important role in inducing the protein aggregation *via* charge–charge interactions.

Previously, the KTKEGV repeats of α-syn were reported to encompass the lipid-binding domain (52). Furthermore, KTKEGV repeats were found to mediate physiological tetramerization and their perturbation caused PD-like neurotoxicity (53). Recently, the structures of α-syn filaments from multiple system atrophy, which is an adult-onset sporadic synucleinopathy with symptoms of parkinsonism (54), were revealed by cryo-EM (5). The additional densities were observed in the front of the side chains of K43, K45, and K58 in the KTKEGV repeats and at the protofilament interface, suggesting the presence of small molecules consisting of phosphate groups. It is possible that negatively charged biomolecules including polyP play a role in the amyloid formation of α-syn through interactions with these repeat motifs *in vivo*. It is also possible that morphologies of α-syn formed at the lower and higher concentrations of polyPs are different because they are formed by distinct mechanisms (Fig. 6). These fibrils were referred to as low and high salt fibrils, respectively (Fig. 6). On the other hand, Melki and colleagues (35, 36), reported that ribbon fibrils consisting of several protofilaments and thick fibrils were formed at low (5 mM Tris-HCl) and high (50 mM Tris-HCl, 150 mM KCl) salt conditions, respectively. We suggest that the polyP concentration-dependent changes in structures and morphologies are useful for understanding distinct α-synucleinopathies (55).

Conclusions

We demonstrated that polyPs accelerate amyloid formation of α-syn at low and high concentrations under neutral pH conditions. PolyPs at low concentrations reduce the solubility of α-syn *via* specific charge–charge interactions with the positively charged N-terminal KTKEGV repeats. In contrast, polyPs at high concentrations reduce the solubility of α-syn *via* Hofmeister salting-out effects. Although the present NMR measurements combined with PCA did not clarify the molecular mechanisms of the polyP effects, *i.e.*, either, (i) specific interactions between tetraP and α-syn, (ii) a backbone conformational change induced in α-syn due to the interaction with tetraP, or (iii) the formation of soluble protein oligomers/aggregates induced due to binding to TetraP, the results clearly separated the two types of effects. Of note, the polyP concentrations associated with the charge–charge interactions are similar to those *in vivo*. Although polyP and negatively charged biopolymers consisting of a large number of phosphate groups are essential elements for organisms, they may play an important role in amyloid fibril formation *in vivo*. Moreover, we previously reported that isoelectric point precipitation is important for inducing α-syn amyloid fibrils upon interaction with negatively charged membranes (50). Therefore, clarifying the biophysical mechanisms of amyloid formation in terms of solubility and supersaturation is essential and complementary to structural analysis for improving our understanding of amyloid fibrils and developing therapeutic strategies.

Experimental procedures

Materials

α-Syn was expressed in *Escherichia coli* BL21(DE3) and purified as previously described (56). The purity of the protein solution was confirmed to be greater than 95% by SDS-PAGE and MALDI-TOF mass spectroscopy (Bruker Daltonics). OrthoP, diP, triP, and tetraP were purchased from Nacalai Tesque. PolyP-S and polyP-L were purchased from Bioenex. ThT was purchased from Wako Pure Chemical Industries, Ltd, and all other reagents were obtained from Nacalai Tesque.

Amyloid formation in the presence of polyPs

α-Syn was dissolved at a final concentration of 0.1 mg/ml in 20 mM sodium phosphate buffer (pH 7.5), 5 μM ThT containing varying concentrations of orthoP, diP, triP, tetraP, polyP-S, polyP-L, or NaCl. The pH was adjusted to 7.0 to 7.5 using NaOH. The concentration of α-syn monomers was measured using the extinction coefficient (ε = 5120 M^{-1} cm^{-1}) at 280 nm based on the amino acid composition (57). Reaction mixtures in 96-well plate were ultrasonicated from three directions (*i.e.*, two sides and the bottom) for 1 min and then incubated for 4 min without ultrasonication using a water bath-type ultrasonic transmitter ELESTEIN 070-GOTW (Elekon). Ultrasonication was repeated and 96-well plate was rotated at 3.3 rpm during incubation at 37 °C. The frequency of the instrument was 17 to 20 kHz and the power output was set to deliver a maximum of approximately 550 W. ThT fluorescence of 96-well plate was measured using an MTP-810 Lab microplate reader (Corona Electric Co) at 37 °C. The excitation and emission wavelengths were 450 and 490 nm, respectively. The lag time for aggregation was defined as the time at which ThT fluorescence or light scattering reached one-tenth of the maximum.

CD measurements

Far-UV CD spectra were measured by a Jasco spectropolarimeter J-720 (Jasco Co, Ltd) using a quartz cell with a light path of 1 mm and a protein concentration of 0.1 mg/ml at 25 °C. The results were expressed as the mean residue ellipticity [θ] (deg cm^2 $dmol^{-1}$).

Solution NMR measurements

^{15}N-uniformly labeled α-syn solutions at 1.0 mg/ml containing 2% D_2O and varying concentrations of tetraP were prepared for 2D ^{1}H-^{15}N HSQC experiments. The pH of the solution was adjusted to 7.0 to 7.4 using NaOH. The spectra were recorded on a Bruker Avance-III 950 MHz spectrometer with a cryogenic probe at 15 °C. Peak assignment was performed by 3D HN(CA)NNH measurement, which is applicable for the signal assignment of IDPs (58). NMR data were processed by TOPSPIN-NMR software and analyzed using Sparky (59). The weighted averages of the ^{1}H and ^{15}N chemical shift changes of α-syn upon the addition of tetraP were calculated by the function $\Delta\delta = [(\Delta\delta_{1H}]^2 + (\Delta\delta_{15N}/8)^2]^{1/2}$ against the residue number.

Principal component analysis (PCA) of ^{1}H-^{15}N HSQC spectra

The chemical shift data for each spectrum were represented as a one-dimensional vector that contains the δ_H and δ_N values. As pretreatment, the δ_N values were divided by 8, and all δ_H and δ_N were subtracted from the average over the measured tetraP concentrations. The vectors were used to build a two-dimensional matrix, in which the rows are the chemical shift data from each spectrum and the columns are the variables of tetraP concentration. The matrix size was [119 (number of traceable residues) × 2 (δ_H and δ_N)] × 11 (tetraP concentrations). PCA of chemical shift data was performed using R (University of Auckland, New Zealand), as described previously (50). In the present case, we obtained nine PCs and corresponding contribution ratios. The scores for each PC were calculated by multiplying the eigenvectors by their corresponding eigenvalues.

TEM observation

A 5-μl aliquot of the sample solution was placed on a collodion-coated copper grid (Nisshin EM Co) for 1 min and excess solution was removed by blotting with filter paper. The grid was negatively stained with a 5-μl droplet of 2% (w/v) phosphotungstic acid for 1 min. The liquid on the grid was removed by blotting and then dried. TEM was performed using an H-7650 transmission electron microscope (HITACHI) operating at an acceleration voltage of 80 kV with a magnification of ×30,000.

Data availability

All data are contained within the article.

Supporting information—This article contains supporting information.

Acknowledgments—This study was performed as part of the Cooperative Research Program for the Institute for Protein Research, Osaka University (CR-18-02) and was supported by the Japan Society for the Promotion of Science (20K06580) and Core-to-Core Program A (Advance Research Networks), Ministry of Education, Culture, Sports, Science and Technology (17H06352), and SENTAN from the Japan Agency for Medical Research and Development, AMED (16809242).

Author contributions—K. Y., M. S., K. I., H. M., and Y. G.: conceptualization; K. Y., M. S., and C. A.: data curation; K. Y., M. S., and C. A.: formal analysis; K. Y., M. S., and C. A.: investigation; K. Y., M. S., and K. I.: methodology; K. Y., Y. G.: writing—original draft; K. Y., Y. G.: visualization; K. Y., M. S., and C. A.: resources; H. M., Y. K., and Y. G.: supervision; K. Y., C. A., and Y. G.: funding acquisition; K. Y., Y. K., and Y. G.: writing—review and editing.

Funding and additional information—C. A. was supported by Grant-in-Aid for JSPS Foreign Fellows.

Conflicts of interest—The authors declare that they have no conflicts of interest with the contents of this article.

Abbreviations—The abbreviations used are: α-syn, α-synuclein; CD, circular dichroism; LS, light scattering; PCA, principal component

analysis; pI, isotropic point; polyP, polyphosphate; TEM, transmission electron microscopy; ThT, thioflavin T.

References

1. Riek, R., and Eisenberg, D. S. (2016) The activities of amyloids from a structural perspective. *Nature* **539**, 227–235
2. Sipe, J. D., Benson, M. D., Buxbaum, J. N., Ikeda, S. I., Merlini, G., Saraiva, M. J., and Westermark, P. (2016) Amyloid fibril proteins and amyloidosis: Chemical identification and clinical classification International Society of Amyloidosis 2016 nomenclature guidelines. *Amyloid* **23**, 209–213
3. Chiti, F., and Dobson, C. M. (2017) Protein misfolding, amyloid formation, and human disease: A summary of progress over the last decade. *Annu. Rev. Biochem.* **86**, 27–68
4. Guerrero-Ferreira, R., Taylor, N. M., Mona, D., Ringler, P., Lauer, M. E., Riek, R., Britschgi, M., and Stahlberg, H. (2018) Cryo-EM structure of alpha-synuclein fibrils. *Elife* **7**, e36402
5. Schweighauser, M., Shi, Y., Tarutani, A., Kametani, F., Murzin, A. G., Ghetti, B., Matsubara, T., Tomita, T., Ando, T., Hasegawa, K., Murayama, S., Yoshida, M., Hasegawa, M., Scheres, S. H. W., and Goedert, M. (2020) Structures of alpha-synuclein filaments from multiple system atrophy. *Nature* **585**, 464–469
6. Iadanza, M. G., Silvers, R., Boardman, J., Smith, H. I., Karamanos, T. K., Debelouchina, G. T., Su, Y., Griffin, R. G., Ranson, N. A., and Radford, S. E. (2018) The structure of a beta2-microglobulin fibril suggests a molecular basis for its amyloid polymorphism. *Nat. Commun.* **9**, 4517
7. Clark, P. L. (2004) Protein folding in the cell: Reshaping the folding funnel. *Trends Biochem. Sci.* **29**, 527–534
8. Baldwin, A. J., Knowles, T. P., Tartaglia, G. G., Fitzpatrick, A. W., Devlin, G. L., Shammas, S. L., Waudby, C. A., Mossuto, M. F., Meehan, S., Gras, S. L., Christodoulou, J., Anthony-Cahill, S. J., Barker, P. D., Vendruscolo, M., and Dobson, C. M. (2011) Metastability of native proteins and the phenomenon of amyloid formation. *J. Am. Chem. Soc.* **133**, 14160–14163
9. Jarrett, J. T., and Lansbury, P. T., Jr. (1993) Seeding "one-dimensional crystallization" of amyloid: A pathogenic mechanism in Alzheimer's disease and scrapie? *Cell* **73**, 1055–1058
10. Ciryam, P., Tartaglia, G. G., Morimoto, R. I., Dobson, C. M., and Vendruscolo, M. (2013) Widespread aggregation and neurodegenerative diseases are associated with supersaturated proteins. *Cell Rep.* **5**, 781–790
11. So, M., Hall, D., and Goto, Y. (2016) Revisiting supersaturation as a factor determining amyloid fibrillation. *Curr. Opin. Struct. Biol.* **36**, 32–39
12. Adachi, M., Noji, M., So, M., Sasahara, K., Kardos, J., Naiki, H., and Goto, Y. (2018) Aggregation-phase diagrams of b2-microglobulin reveal temperature and salt effects on competitive formation of amyloids versus amorphous aggregates. *J. Biol. Chem.* **293**, 14775–14785
13. Noji, M., Sasahara, K., Yamaguchi, K., So, M., Sakurai, K., Kardos, J., Naiki, H., and Goto, Y. (2019) Heating during agitation of b2-microglobulin reveals that supersaturation breakdown is required for amyloid fibril formation at neutral pH. *J. Biol. Chem.* **294**, 15826–15835
14. Munishkina, L. A., Henriques, J., Uversky, V. N., and Fink, A. L. (2004) Role of protein-water interactions and electrostatics in alpha-synuclein fibril formation. *Biochemistry* **43**, 3289–3300
15. Giehm, L., Oliveira, C. L., Christiansen, G., Pedersen, J. S., and Otzen, D. E. (2010) SDS-induced fibrillation of alpha-synuclein: An alternative fibrillation pathway. *J. Mol. Biol.* **401**, 115–133
16. Fusco, G., De Simone, A., Gopinath, T., Vostrikov, V., Vendruscolo, M., Dobson, C. M., and Veglia, G. (2014) Direct observation of the three regions in alpha-synuclein that determine its membrane-bound behaviour. *Nat. Commun.* **5**, 3827
17. Fonseca-Ornelas, L., Eisbach, S. E., Paulat, M., Giller, K., Fernandez, C. O., Outeiro, T. F., Becker, S., and Zweckstetter, M. (2014) Small molecule-mediated stabilization of vesicle-associated helical alpha-synuclein inhibits pathogenic misfolding and aggregation. *Nat. Commun.* **5**, 5857
18. Sawada, M., Yamaguchi, K., Hirano, M., Noji, M., So, M., Otzen, D., Kawata, Y., and Goto, Y. (2020) Amyloid formation of alpha-synuclein based on the solubility- and supersaturation-dependent mechanism. *Langmuir* **36**, 4671–4681
19. Uversky, V. N., Li, J., and Fink, A. L. (2001) Metal-triggered structural transformations, aggregation, and fibrillation of human alpha-synuclein. A possible molecular NK between Parkinson's disease and heavy metal exposure. *J. Biol. Chem.* **276**, 44284–44296
20. Kumble, K. D., and Kornberg, A. (1995) Inorganic polyphosphate in mammalian cells and tissues. *J. Biol. Chem.* **270**, 5818–5822
21. Xie, L., and Jakob, U. (2019) Inorganic polyphosphate, a multifunctional polyanionic protein scaffold. *J. Biol. Chem.* **294**, 2180–2190
22. Hsieh, P. C., Shenoy, B. C., Jentoft, J. E., and Phillips, N. F. (1993) Purification of polyphosphate and ATP glucose phosphotransferase from Mycobacterium tuberculosis H37Ra: Evidence that poly(P) and ATP glucokinase activities are catalyzed by the same enzyme. *Protein Expr. Purif.* **4**, 76–84
23. Muller, F., Mutch, N. J., Schenk, W. A., Smith, S. A., Esterl, L., Spronk, H. M., Schmidbauer, S., Gahl, W. A., Morrissey, J. H., and Renne, T. (2009) Platelet polyphosphates are proinflammatory and procoagulant mediators *in vivo*. *Cell* **139**, 1143–1156
24. Abramov, A. Y., Fraley, C., Diao, C. T., Winkfein, R., Colicos, M. A., Duchen, M. R., French, R. J., and Pavlov, E. (2007) Targeted polyphosphatase expression alters mitochondrial metabolism and inhibits calcium-dependent cell death. *Proc. Natl. Acad. Sci. U. S. A.* **104**, 18091–18096
25. Ishige, K., Zhang, H., and Kornberg, A. (2002) Polyphosphate kinase (PPK2), a potent, polyphosphate-driven generator of GTP. *Proc. Natl. Acad. Sci. U. S. A.* **99**, 16684–16688
26. Ito, T., Yamamoto, S., Yamaguchi, K., Sato, M., Kaneko, Y., Goto, S., Goto, Y., and Narita, I. (2020) Inorganic polyphosphate potentiates lipopolysaccharide-induced macrophage inflammatory response. *J. Biol. Chem.* **295**, 4014–4023
27. Cremers, C. M., Knoefler, D., Gates, S., Martin, N., Dahl, J. U., Lempart, J., Xie, L., Chapman, M. R., Galvan, V., Southworth, D. R., and Jakob, U. (2016) Polyphosphate: A conserved modifier of amyloidogenic processes. *Mol. Cell* **63**, 768–780
28. Zhang, C. M., Yamaguchi, K., So, M., Sasahara, K., Ito, T., Yamamoto, S., Narita, I., Kardos, J., Naiki, H., and Goto, Y. (2019) Possible mechanisms of polyphosphate-induced amyloid fibril formation of beta2-microglobulin. *Proc. Natl. Acad. Sci. U. S. A.* **116**, 12833–12838
29. Wang, X., Shi, C., Mo, J., Xu, Y., Wei, W., and Zhao, J. (2020) An inorganic biopolymer polyphosphate controls positively charged protein phase transitions. *Angew. Chem. Int. Ed. Engl.* **59**, 2679–2683
30. Noji, M., So, M., Yamaguchi, K., Hojo, H., Onda, M., Akazawa-Ogawa, Y., Hagihara, Y., and Goto, Y. (2018) Heat-induced aggregation of hen ovalbumin suggests a key factor responsible for serpin polymerization. *Biochemistry* **57**, 5415–5426
31. Sasahara, K., Yamaguchi, K., So, M., and Goto, Y. (2019) Polyphosphates diminish solubility of a globular protein and thereby promote amyloid aggregation. *J. Biol. Chem.* **294**, 15318–15329
32. Wilhelm, B. G., Mandad, S., Truckenbrodt, S., Krohnert, K., Schafer, C., Rammner, B., Koo, S. J., Classen, G. A., Krauss, M., Haucke, V., Urlaub, H., and Rizzoli, S. O. (2014) Composition of isolated synaptic boutons reveals the amounts of vesicle trafficking proteins. *Science* **344**, 1023–1028
33. Cohlberg, J. A., Li, J., Uversky, V. N., and Fink, A. L. (2002) Heparin and other glycosaminoglycans stimulate the formation of amyloid fibrils from alpha-synuclein *in vitro*. *Biochemistry* **41**, 1502–1511
34. Terakawa, M. S., Lee, Y. H., Kinoshita, M., Lin, Y., Sugiki, T., Fukui, N., Ikenoue, T., Kawata, Y., and Goto, Y. (2018) Membrane-induced initial structure of alpha-synuclein control its amyloidogenesis on model membranes. *Biochim. Biophys. Acta Biomembr.* **1860**, 757–766
35. Bousset, L., Pieri, L., Ruiz-Arlandis, G., Gath, J., Jensen, P. H., Habenstein, B., Madiona, K., Olieric, V., Bockmann, A., Meier, B. H., and Melki, R. (2013) Structural and functional characterization of two alpha-synuclein strains. *Nat. Commun.* **4**, 2575
36. Melki, R. (2015) Role of different alpha-synuclein strains in synucleinopathies, similarities with other neurodegenerative diseases. *J. Parkinsons Dis.* **5**, 217–227

37. Jaumot, J., Vives, M., and Gargallo, R. (2004) Application of multivariate resolution methods to the study of biochemical and biophysical processes. *Anal. Biochem.* **327**, 1–13
38. Sakurai, K., and Goto, Y. J. (2007) Principal component analysis of the pH-dependent conformational transitions of bovine beta-lactoglobulin monitored by heteronuclear NMR. *Proc. Natl. Acad. Sci. U. S. A.* **104**, 15346–15351
39. Lever, J., Krzywinski, M., and Atman, N. (2017) POINTS OF SIGNIFICANCE principal component analysis. *Nat. Methods* **14**, 641–642
40. Kjaergaard, M., Brander, S., and Poulsen, F. M. (2011) Random coil chemical shift for intrinsically disordered proteins: Effects of temperature and pH. *J. Biomol. NMR* **49**, 139–149
41. Lager, G. A., and Gibbs, G. V. (1973) Effect of variations in O-P-O and P-O-P angles on P-O bond overlap populations for some selected orthophosphates and pyrophosphates. *Am. Mineral.* **58**, 756–764
42. Theillet, F. X., Binolfi, A., Bekei, B., Martorana, A., Rose, H. M., Stuiver, M., Verzini, S., Lorenz, D., van Rossum, M., Goldfarb, D., and Selenko, P. (2016) Structural disorder of monomeric alpha-synuclein persists in mammalian cells. *Nature* **530**, 45–50
43. Yoshimura, Y., Holmberg, M. A., Kukic, P., Andersen, C. B., Mata-Cabana, A., Falsone, S. F., Vendruscolo, M., Nollen, E. A. A., and Mulder, F. A. A. (2017) MOAG-4 promotes the aggregation of alpha-synuclein by competing with self-protective electrostatic interactions. *J. Biol. Chem.* **292**, 8269–8278
44. Raman, B., Chatani, E., Kihara, M., Ban, T., Sakai, M., Hasegawa, K., Naiki, H., Rao Ch, M., and Goto, Y. (2005) Critical balance of electrostatic and hydrophobic interactions is required for beta 2-microglobulin amyloid fibril growth and stability. *Biochemistry* **44**, 1288–1299
45. Nitani, A., Muta, H., Adachi, M., So, M., Sasahara, K., Sakurai, K., Chatani, E., Naoe, K., Ogi, H., Hall, D., and Goto, Y. (2017) Heparin-dependent aggregation of hen egg white lysozyme reveals two distinct mechanisms of amyloid fibrillation. *J. Biol. Chem.* **292**, 21219–21230
46. So, M., Hata, Y., Naiki, H., and Goto, Y. (2017) Heparin-induced amyloid fibrillation of b2 -microglobulin explained by solubility and a supersaturation-dependent conformational phase diagram. *Protein Sci.* **26**, 1024–1036
47. Collins, K. D., and Washabaugh, M. W. (1985) The Hofmeister effect and the behaviour of water at interfaces. *Q. Rev. Biophys.* **18**, 323–422
48. Nihonyanagi, S., Yamaguchi, S., and Tahara, T. (2014) Counterion effect on interfacial water at charged interfaces and its relevance to the Hofmeister series. *J. Am. Chem. Soc.* **136**, 6155–6158
49. Marek, P. J., Patsalo, V., Green, D. F., and Raleigh, D. P. (2012) Ionic strength effects on amyloid formation by amylin are a complicated interplay among Debye screening, ion selectivity, and Hofmeister effects. *Biochemistry* **51**, 8478–8490
50. Furukawa, K., Aguirre, C., So, M., Sasahara, K., Miyanoiri, Y., Sakurai, K., Yamaguchi, K., Ikenaka, K., Mochizuki, H., Kardos, J., Kawata, Y., and Goto, Y. (2020) Isoelectric point-amyloid formation of a-synuclein extends the solubility and supersaturation-limited mechanism. *Curr. Res. Struct. Biol.* **2**, 35–44
51. Ruiz, F. A., Lea, C. R., Oldfield, E., and Docampo, R. (2004) Human platelet dense granules contain polyphosphate and are similar to acidocalcisomes of bacteria and unicellular eukaryotes. *J. Biol. Chem.* **279**, 44250–44257
52. Davidson, W. S., Jonas, A., Clayton, D. F., and George, J. M. (1998) Stabilization of alpha-synuclein secondary structure upon binding to synthetic membranes. *J. Biol. Chem.* **273**, 9443–9449
53. Dettmer, U., Newman, A. J., von Saucken, V. E., Bartels, T., and Selkoe, D. (2015) KTKEGV repeat motifs are key mediators of normal alpha-synuclein tetramerization: Their mutation causes excess monomers and neurotoxicity. *Proc. Natl. Acad. Sci. U. S. A.* **112**, 9596–9601
54. Graham, J. G., and Oppenheimer, D. R. (1969) Orthostatic hypotension and nicotine sensitivity in a case of multiple system atrophy. *J. Neurol. Neurosurg. Psychiatry* **32**, 28–34
55. Strohaker, T., Jung, B. C., Liou, S. H., Fernandez, C. O., Riedel, D., Becker, S., Halliday, G. M., Bennati, M., Kim, W. S., Lee, S. J., and Zweckstetter, M. (2019) Structural heterogeneity of alpha-synuclein fibrils amplified from patient brain extracts. *Nat. Commun.* **10**, 5535
56. Yagi, H., Kusaka, E., Hongo, K., Mizobata, T., and Kawata, Y. (2005) Amyloid fibril formation of alpha-synuclein is accelerated by preformed amyloid seeds of other proteins: Implications for the mechanism of transmissible conformational diseases. *J. Biol. Chem.* **280**, 38609–38616
57. Gill, S. C., and von Hippel, P. H. (1989) Calculation of protein extinction coefficients from amino acid sequence data. *Anal. Biochem.* **182**, 319–326
58. Weisemann, R., Ruterjans, H., and Bermel, W. (1993) 3D triple-resonance NMR techniques for the sequential assignment of NH and 15N resonances in 15N- and 13C-labelled proteins. *J. Biomol. NMR* **3**, 113–120
59. Lee, W., Tonelli, M., and Markley, J. L. (2015) NMRFAM-SPARKY: Enhanced software for biomolecular NMR spectroscopy. *Bioinformatics* **31**, 1325–1327
60. Kyte, J., and Doolittle, R. F. (1982) A simple method for displaying the hydropathic character of a protein. *J. Mol. Biol.* **157**, 105–132